

Kibble-Zurek mechanism in a quenched ferromagnetic Bose-Einstein condensate

Hiroki Saito¹, Yuki Kawaguchi², and Masahito Ueda^{2,3}

¹*Department of Applied Physics and Chemistry, The University of Electro-Communications, Tokyo 182-8585, Japan*

²*Department of Physics, Tokyo Institute of Technology, Tokyo 152-8551, Japan*

³*Macroscopic Quantum Control Project, ERATO, JST, Bunkyo-ku, Tokyo 113-8656, Japan*

(Dated: October 31, 2018)

The spin vortices are shown to be created through the Kibble-Zurek (KZ) mechanism in a quantum phase transition of a spin-1 ferromagnetic Bose-Einstein condensate, when the applied magnetic field is quenched below a critical value. It is shown that the magnetic correlation functions have finite correlation lengths, and magnetizations at widely separated positions grow in random directions, resulting in spin vortices. We numerically confirm the scaling law that the winding number of spin vortices is proportional to the square root of the length of the closed path, and for slow quench, proportional to $\tau_Q^{-1/6}$ with τ_Q being the quench time. The relation between the spin conservation and the KZ mechanism is discussed.

PACS numbers: 03.75.Mn, 03.75.Lm, 73.43.Nq, 64.60.Ht

I. INTRODUCTION

Spontaneous symmetry breaking in a phase transition produces local domains of an order parameter. If domains are separated by such a long distance that they cannot exchange information, local domains grow initially with random phases and eventually give rise to topological defects when they overlap. This scenario of topological-defect formation in continuous-symmetry breaking is known as the Kibble-Zurek (KZ) mechanism [1, 2], which originally predicted the cosmic-string and monopole formation in the early Universe [1], and has since been applied to a wide variety of systems. Experimentally, the KZ mechanism has been examined in liquid crystals [3, 4], superfluid ⁴He [5] and ³He [6, 7], an optical Kerr medium [8], Josephson junctions [9, 10], and superconducting films [11].

Recently, spontaneous magnetization in a spinor Bose-Einstein condensate (BEC) has attracted much interest as a new system for studying the KZ mechanism [12, 13, 14, 15]. In the experiment performed by the Berkeley group [12], a BEC of $F = 1$ ⁸⁷Rb atoms are prepared in the $m = 0$ state, where F is the hyperfine spin and m is its projection on the direction of the magnetic field. By quench of the magnetic field, say in the z direction, magnetization appears in the x - y plane. Since the spinor Hamiltonian is axisymmetric with respect to the z axis, the magnetization in the x - y direction breaks the U(1) symmetry in the spin space. Thus, local domain formation is expected to lead to topological defects — spin vortices — through the KZ mechanism.

However, the origin of the spin vortices observed after the quench in the Berkeley experiment [12] cannot be attributed to the KZ mechanism. In fact, in Ref. [12], the spin correlation extends over the entire system (at least in the x direction) and the domains are not independent with each other. We have shown in Ref. [13] that the origin of the observed spin vortices is initial spin correlation due to the residual $m = \pm 1$ atoms, which forms domain structure followed by spin vortex creation [16]. In order

to realize the KZ mechanism in this system, i.e., in order to ensure that the magnetic domains grow independently, the size of the system must be much larger than the spin correlation length and the long-range correlation in the initial spin state must be absent. The aim of the present paper is to show that under these conditions spin vortices are generated through the KZ mechanism.

In the present paper we will consider 1D-ring and 2D-disk geometries. We will show that in the 1D ring the average spin winding number after the quench is proportional to the square root of the system size, which is in agreement with the KZ prediction [2]. In 2D the winding number along a path with radius R is also proportional to $R^{1/2}$ as long as R is much larger than the vortex spacing, while it is proportional to R for small R . When the magnetic field is quenched slowly, the winding number is shown to be proportional to $\tau_Q^{-1/6}$ with τ_Q being the quench time. This power law can be understood by Zurek's simple discussion [2].

The spinor BEC is different from the other systems in which the KZ mechanism has been observed, in that the total spin is conserved when the quadratic Zeeman energy q is negligible. This fact is seemingly incompatible with the KZ postulate, since the magnetic domains must be correlated with each other so that the total magnetization vanishes. We will show that for $q = 0$ small magnetic domains are aligned to cancel out the local spin averaged over the correlation length, and that they are independent with each other over a greater length scale; the spin conservation is thus compatible with the KZ mechanism.

The present paper is organized as follows. Section II analyzes spontaneous magnetization of a spin-1 BEC and the resultant magnetic correlation functions using the Bogoliubov approximation. Section III performs numerical simulations of the dynamics of quenched BECs in 1D and 2D, and shows that the KZ mechanism does emerge in the present system. Section IV provides conclusions.

II. BOGOLIUBOV ANALYSIS OF A QUENCHED FERROMAGNETIC BOSE-EINSTEIN CONDENSATE

A. Hamiltonian for the spin-1 atoms

We consider spin-1 bosonic atoms with mass M confined in a potential $V_{\text{trap}}(\mathbf{r})$. The noninteracting part of the Hamiltonian is given by

$$\hat{H}_0 = \int d\mathbf{r} \sum_{m=-1}^1 \hat{\psi}_m^\dagger(\mathbf{r}) \left[-\frac{\hbar^2}{2M} \nabla^2 + V_{\text{trap}}(\mathbf{r}) \right] \hat{\psi}_m(\mathbf{r}), \quad (1)$$

where $\hat{\psi}_m(\mathbf{r})$ annihilates an atom in magnetic sublevel m of spin at a position \mathbf{r} .

The interaction between atoms with s -wave scattering is described by

$$\hat{H}_{\text{int}} = \frac{1}{2} \int d\mathbf{r} : \left[c_0 \hat{\rho}^2(\mathbf{r}) + c_1 \hat{\mathbf{F}}^2(\mathbf{r}) \right] :, \quad (2)$$

where the symbol $::$ denotes the normal order and

$$\hat{\rho}(\mathbf{r}) = \sum_{m=-1}^1 \hat{\psi}_m^\dagger(\mathbf{r}) \hat{\psi}_m(\mathbf{r}), \quad (3)$$

$$\hat{\mathbf{F}}(\mathbf{r}) = \sum_{m,m'} \hat{\psi}_m^\dagger(\mathbf{r}) \mathbf{f}_{mm'} \hat{\psi}_{m'}(\mathbf{r}), \quad (4)$$

with $\mathbf{f} = (f_x, f_y, f_z)$ being the spin-1 matrices. The interaction coefficients in Eq. (2) are given by

$$c_0 = \frac{4\pi\hbar^2}{M} \frac{a_0 + 2a_2}{3}, \quad (5a)$$

$$c_1 = \frac{4\pi\hbar^2}{M} \frac{a_2 - a_0}{3}, \quad (5b)$$

where a_S is the s -wave scattering lengths for two colliding atoms with total spin S .

When magnetic field \mathbf{B} is applied, the linear Zeeman effect rotates the spin around the direction of \mathbf{B} at the Larmor frequency. Since \hat{H}_0 and \hat{H}_{int} are spin-rotation invariant and we assume the uniform magnetic field, the linear Zeeman term has only a trivial effect on spin dynamics — uniform rotation of spins about \mathbf{B} — which is therefore ignored. The quadratic Zeeman effects for an $F = 1$ ^{87}Rb atom is described by

$$\hat{H}_q = \frac{\mu_B^2}{4E_{\text{hf}}} \int d\mathbf{r} \sum_{m,m'} \hat{\psi}_m^\dagger(\mathbf{r}) [(\mathbf{B} \cdot \mathbf{f})^2]_{mm'} \hat{\psi}_{m'}(\mathbf{r}), \quad (6)$$

where μ_B is the Bohr magneton and $E_{\text{hf}} > 0$ is the hyperfine splitting energy between $F = 1$ and $F = 2$. The total Hamiltonian is given by the sum of Eqs. (1), (2), and (6),

$$\hat{H} = \hat{H}_0 + \hat{H}_q + \hat{H}_{\text{int}}. \quad (7)$$

B. Time evolution in the Bogoliubov approximation

In the initial state, all atoms are prepared in the $m = 0$ state. We study the spin dynamics of the system using the Bogoliubov approximation with respect to this initial state. For simplicity, we assume $V_{\text{trap}} = 0$ in this section.

In the Bogoliubov approximation, the BEC part in the field operator is replaced by a c -number. In the present case, we write the $m = 0$ component of the field operator as

$$\hat{\psi}_0(\mathbf{r}) = e^{-ic_0 n t / \hbar} \left[\sqrt{n} + \delta\hat{\psi}_0(\mathbf{r}) \right], \quad (8)$$

where n is the atomic density. We expand $\hat{\psi}_{\pm 1}(\mathbf{r})$ as

$$\hat{\psi}_{\pm 1}(\mathbf{r}) = e^{-ic_0 n t / \hbar} \sum_{\mathbf{k}} \frac{1}{\sqrt{V}} e^{i\mathbf{k} \cdot \mathbf{r}} \hat{a}_{\pm 1, \mathbf{k}}, \quad (9)$$

where V is the volume of the system and $\hat{a}_{\pm 1, \mathbf{k}}$ is the annihilation operator of an atom in the $m = \pm 1$ state with wave vector \mathbf{k} . Keeping only up to the second order of $\delta\hat{\psi}_0(\mathbf{r})$ and $\hat{\psi}_{\pm 1}(\mathbf{r})$ in the Hamiltonian, we obtain the Heisenberg equation of motion for $\hat{a}_{\pm 1, \mathbf{k}}$ as

$$i\hbar \frac{d\hat{a}_{\pm 1, \mathbf{k}}(t)}{dt} = (\varepsilon_{\mathbf{k}} + q + c_1 n) \hat{a}_{\pm 1, \mathbf{k}}(t) + c_1 n \hat{a}_{\mp 1, -\mathbf{k}}^\dagger(t), \quad (10)$$

where $\varepsilon_{\mathbf{k}} = \hbar^2 k^2 / (2M)$ and $q = \mu_B^2 B^2 / (4E_{\text{hf}})$. The magnetic field is assumed to be applied in the z direction. The solution of Eq. (10) is obtained as

$$\begin{aligned} \hat{a}_{\pm 1, \mathbf{k}}(t) = & \left(\cos \frac{E_{\mathbf{k}} t}{\hbar} - i \frac{\varepsilon_{\mathbf{k}} + q + c_1 n}{E_{\mathbf{k}}} \sin \frac{E_{\mathbf{k}} t}{\hbar} \right) \hat{a}_{\pm 1, \mathbf{k}}(0) \\ & - \left(i \frac{c_1 n}{E_{\mathbf{k}}} \sin \frac{E_{\mathbf{k}} t}{\hbar} \right) \hat{a}_{\mp 1, -\mathbf{k}}^\dagger(0), \end{aligned} \quad (11)$$

where

$$E_{\mathbf{k}} = \sqrt{(\varepsilon_{\mathbf{k}} + q)(\varepsilon_{\mathbf{k}} + q + 2c_1 n)}. \quad (12)$$

When $E_{\mathbf{k}}$ is imaginary, the corresponding modes are dynamically unstable and grow exponentially. Since $c_1 < 0$ and $q > 0$ for $F = 1$ ^{87}Rb atoms, the exponential growth occurs for

$$q < 2|c_1|n \equiv q_c. \quad (13)$$

This critical value of q agrees with the phase boundary between the polar phase and the broken-axisymmetry phase [17, 18]. When $q \leq q_c/2$, the wave number of the most unstable mode is

$$k_{\text{mu}} = \pm \sqrt{\frac{2M}{\hbar^2} \left(\frac{q_c}{2} - q \right)}, \quad (14)$$

and when $q_c/2 < q < q_c$, $k_{\text{mu}} = 0$.

C. Fast quench

We consider the situation in which q is much larger than the other characteristic energies for $t < 0$, and q is suddenly quenched below q_c at $t = 0$. During $t < 0$, the time evolution in Eq. (11) is $\hat{a}_{\pm 1, \mathbf{k}}(t) \simeq e^{-iqt/\hbar} \hat{a}_{\pm 1, \mathbf{k}}(0)$, and the $m = \pm 1$ state remains in the vacuum state. For $t > 0$, we obtain the time evolution of the density of the $m = \pm 1$ component as

$$\begin{aligned} \langle \hat{\psi}_{\pm 1}^\dagger(\mathbf{r}, t) \hat{\psi}_{\pm 1}(\mathbf{r}, t) \rangle &= \frac{1}{V} \sum_{\mathbf{k}} \left| \frac{c_1 n}{E_k} \sin \frac{E_k t}{\hbar} \right|^2 \\ &\simeq \frac{1}{V} \sum_{k < k_c} \frac{q_c^2}{16|E_k|^2} e^{2|E_k|t/\hbar} \end{aligned} \quad (15)$$

where the expectation value is taken with respect to the vacuum state of the $m = \pm 1$ component. In the second line of Eq. (15), we have kept the unstable modes alone with $k < k_c \equiv \sqrt{2M(q_c - q)}/\hbar$ by assuming that $|E_k|t/\hbar \gg 1$. This result indicates that the $m = \pm 1$ components grow exponentially after the quench.

Since the operator $\hat{\psi}_0$ in Eq. (4) is replaced by \sqrt{n} in the Bogoliubov approximation, the magnetization operator $\hat{F}_+ = \hat{F}_-^\dagger = \hat{F}_x + i\hat{F}_y$ has the form,

$$\hat{F}_+(\mathbf{r}) = \sqrt{2n} \left[\hat{\psi}_1^\dagger(\mathbf{r}) + \hat{\psi}_{-1}(\mathbf{r}) \right]. \quad (16)$$

Using Eq. (11), the time evolution of the correlation function is calculated to be

$$\begin{aligned} &\langle \hat{F}_+(\mathbf{r}, t) \hat{F}_-(\mathbf{r}', t) \rangle \\ &= \frac{2n}{V} \sum_{\mathbf{k}} \left| \cos \frac{E_k t}{\hbar} + i \frac{\varepsilon_k + q}{E_k} \sin \frac{E_k t}{\hbar} \right|^2 e^{i\mathbf{k} \cdot (\mathbf{r} - \mathbf{r}')} \\ &\simeq \frac{n}{2V} \sum_{k < k_c} \frac{q_c}{q_c - q - \varepsilon_k} e^{2|E_k|t/\hbar + i\mathbf{k} \cdot (\mathbf{r} - \mathbf{r}')}, \end{aligned} \quad (17a)$$

$$\simeq \frac{n}{2V} \sum_{k < k_c} \frac{q_c}{q_c - q - \varepsilon_k} e^{2|E_k|t/\hbar + i\mathbf{k} \cdot (\mathbf{r} - \mathbf{r}')}, \quad (17b)$$

where in the second line we have kept the unstable modes alone.

From the exponential factor in Eq. (17b), we see that the sum is contributed mostly from \mathbf{k} around the mode with maximum $|E_k|$. The denominator in the summand of Eq. (17b) is much smoother than the exponential factor if q is not close to q_c , and then we approximate ε_k with $\varepsilon_{\text{mu}} = \hbar^2 k_{\text{mu}}^2 / (2M)$ in the denominator. We expand $2|E_k|t/\hbar$ around k_{mu} in the exponent as

$$\frac{2|E_k|t}{\hbar} = \frac{t}{\tau} \left(1 - \frac{1}{4} \xi^2 \Delta k^2 - \frac{1}{256} \Xi^4 \Delta k^4 \right) + O(\Delta k^6), \quad (18)$$

where $\Delta k = k - k_{\text{mu}}$. It is clear that τ sets the time scale for the exponential growth. The magnetization is observed when it sufficiently grows, i.e., $t \sim \tau$. Replacing the summation with the Gaussian integral in Eq. (17b),

we find that ξ represents the correlation length. For $q < q_c/2$, k_{mu} is given by Eq. (14), and

$$\tau = \frac{\hbar}{q_c}, \quad (19)$$

$$\xi = \sqrt{\frac{8\hbar^2 q_c - 2q}{M q_c^2}}. \quad (20)$$

For $q_c/2 < q < q_c$, $k_{\text{mu}} = 0$ and

$$\tau = \frac{\hbar}{2\sqrt{q(q_c - q)}}, \quad (21)$$

$$\xi = \sqrt{\frac{\hbar^2}{M} \frac{2q - q_c}{q(q_c - q)}}. \quad (22)$$

At $q = q_c/2$, Eqs. (20) and (22) vanish, and the Δk^4 term in Eq. (18) becomes important, with

$$\Xi = 4 \left(\frac{\hbar^4}{2M^2 q_c^2} \right)^{1/4}. \quad (23)$$

We first consider a 1D system with the periodic boundary condition, i.e., the 1D ring geometry. We assume that the radius of the ring R is much larger than the domain size, and the curvature of the ring does not affect the dynamics.

For $q < q_c/2$, the magnetic correlation function is calculated to be

$$\begin{aligned} \langle \hat{F}_+(\theta, t) \hat{F}_-(\theta', t) \rangle &= \frac{2n}{\xi} \sqrt{\frac{\tau}{\pi t}} \cos[k_{\text{mu}} R(\theta - \theta')] \\ &\times e^{t/\tau - \tau R^2(\theta - \theta')^2 / (t\xi^2)}, \end{aligned} \quad (24)$$

where τ and ξ are given by Eqs. (19) and (20), and θ and θ' are azimuthal angles. For $q_c/2 < q < q_c$, we obtain

$$\langle \hat{F}_+(\theta, t) \hat{F}_-(\theta', t) \rangle = \frac{n}{2\xi} \sqrt{\frac{\tau}{\pi t}} \frac{q_c}{q_c - q} e^{t/\tau - \tau R^2(\theta - \theta')^2 / (t\xi^2)} \quad (25)$$

with Eqs. (21) and (22). At $q = q_c/2$, the correlation function reads

$$\begin{aligned} &\langle \hat{F}_+(\theta, t) \hat{F}_-(\theta', t) \rangle = \\ &\frac{n}{2\pi\Xi} \frac{q_c}{q_c - q} \left(\frac{\tau}{t} \right)^{1/4} e^{t/\tau} \left[\Gamma\left(\frac{1}{4}\right) {}_0F_2\left(\frac{1}{2}, \frac{3}{4}, \frac{\tau R^4(\theta - \theta')^4}{t\Xi^4}\right) \right. \\ &\left. - 8\sqrt{\frac{\tau}{t}} \frac{R^2(\theta - \theta')^2}{\Xi^2} \Gamma\left(\frac{3}{4}\right) {}_0F_2\left(\frac{5}{4}, \frac{3}{2}, \frac{\tau R^4(\theta - \theta')^4}{t\Xi^4}\right) \right], \end{aligned} \quad (26)$$

where Γ is the Gamma function and

$${}_0F_2(a, b, z) = \sum_{j=0}^{\infty} \frac{\Gamma(a)\Gamma(b)}{\Gamma(a+j)\Gamma(b+j)} \frac{z^j}{j!} \quad (27)$$

is the generalized hypergeometric function. Equation (26) is shown in Fig. 2(a), where Ξ gives a characteristic width of the correlation function.

Next, we consider the 2D geometry. For $q_c/2 < q < q_c$, and then $k_{\text{mu}} = 0$, the integral can be performed analytically, giving

$$\left\langle \hat{F}_+(\mathbf{r}, t) \hat{F}_-(\mathbf{r}', t) \right\rangle = \frac{n\tau}{2\pi\xi^2 t} \frac{q_c}{q_c - q} e^{t/\tau - \tau|\mathbf{r} - \mathbf{r}'|^2/(t\xi^2)}, \quad (28)$$

where τ and ξ are given in Eqs. (21) and (22). For other q , we can perform only the angular integral as

$$\begin{aligned} \left\langle \hat{F}_+(\mathbf{r}, t) \hat{F}_-(\mathbf{r}', t) \right\rangle &= \frac{n}{4\pi} \frac{q_c}{q_c - q - \varepsilon_{\text{mu}}} \\ &\times \int_0^\infty k J_0(k|\mathbf{r} - \mathbf{r}'|) e^{2|E_k|t/\hbar} dk, \end{aligned} \quad (29)$$

where J_0 is the Bessel function. If the exponential factor is much sharper than the Bessel function around k_{mu} , the correlation function (29) is approximated to be $\propto J_0(k_{\text{mu}}|\mathbf{r} - \mathbf{r}'|)$ [14, 15].

As shown above, the correlation function (17b) has a finite correlation length, and the magnetization at positions widely separated from each other grow with independent directions in the x - y plane. Thus, the growth of the magnetic domains is expected to leave topological defects through the KZ mechanism.

D. Slow quench

In the previous sections, we have assumed that the magnetic field is suddenly quenched to the desired value at $t = 0$ and q is held constant for $t > 0$. We assume here that for $t > 0$ the magnetic field is gradually quenched as

$$q(t) = q_c \left(1 - \frac{t}{\tau_Q} \right). \quad (30)$$

The magnetic correlation can be estimated to be

$$\begin{aligned} &\left\langle \hat{F}_+(\mathbf{r}, t) \hat{F}_-(\mathbf{r}', t) \right\rangle \\ &\propto \int d\mathbf{k} \exp \left[\int \frac{2|E_k(t)|t}{\hbar} dt + i\mathbf{k} \cdot (\mathbf{r} - \mathbf{r}') \right]. \end{aligned} \quad (31)$$

Since we are interested in the vicinity of the critical point where correlation starts to grow, we expand $|E_k(t)|$ around $k_{\text{mu}} = 0$ and keep the terms up to the order of k^2 . For the 1D ring, we obtain

$$\left\langle \hat{F}_+(\theta, t) \hat{F}_-(\theta', t) \right\rangle \propto e^{f(t) - R^2(\theta - \theta')^2/\xi_Q^2}, \quad (32)$$

and for the 2D geometry,

$$\left\langle \hat{F}_+(\mathbf{r}, t) \hat{F}_-(\mathbf{r}', t) \right\rangle \propto e^{f(t) - |\mathbf{r} - \mathbf{r}'|^2/\xi_Q^2}, \quad (33)$$

where

$$f(t) = \frac{\tau_Q q_c}{2\hbar} \left[\tan^{-1} \sqrt{\frac{t}{\tau_Q - t}} - \sqrt{\frac{t}{\tau_Q} \left(1 - \frac{t}{\tau_Q} \right) \left(1 - \frac{2t}{\tau_Q} \right)} \right], \quad (34)$$

$$\xi_Q = \left[\frac{4\hbar}{M} \sqrt{t(\tau_Q - t)} \right]^{1/2}. \quad (35)$$

For $t \ll \tau_Q$, $f(t)$ can be expanded as

$$f(t) = \frac{\tau_Q q_c}{2\hbar} \left[\frac{8}{3} \frac{t^{3/2}}{\tau_Q^{3/2}} + O\left(\frac{t^{5/2}}{\tau_Q^{5/2}}\right) \right], \quad (36)$$

and from $f(t) \sim 1$, the time scale for magnetization is given by

$$t_Q \sim \left(\frac{\hbar}{q_c} \right)^{2/3} \tau_Q^{1/3}. \quad (37)$$

Substitution of t_Q into Eq. (35) yields

$$\xi_Q \sim \left(\frac{\hbar^4}{M^3 q_c} \right)^{1/6} \tau_Q^{1/3}. \quad (38)$$

The same power law is obtained in Ref. [14].

It is interesting to note that the results (37) and (38) are easily obtained also by the simple discussion by Zurek [2]. Since $q(t)$ depends on time, τ and ξ given in Eqs. (21) and (22) are time dependent, and hence they are regarded as the growth time and correlation length at each instant of time. The local magnetization is developed after a time t_Q has elapsed such that

$$\tau(t_Q) \sim t_Q. \quad (39)$$

Using

$$\tau(t) = \frac{\hbar\tau_Q}{2q_c\sqrt{t(\tau_Q - t)}} \simeq \frac{\hbar\sqrt{\tau_Q}}{2q_c\sqrt{t}}, \quad (40)$$

we obtain t_Q in Eq. (37). Substituting this t_Q into

$$\xi^2(t) = \frac{\hbar^2}{Mq_c} \frac{\tau_Q - 2t}{t(\tau_Q - t)} \simeq \frac{\hbar^2\tau_Q}{Mq_c t} \quad (41)$$

yields Eq. (38).

III. NUMERICAL SIMULATIONS AND THE KIBBLE-ZUREK MECHANISM

A. Gross-Pitaevskii equation with quantum fluctuations

The multicomponent Gross-Pitaevskii (GP) equation is obtained by replacing the field operators $\hat{\psi}_m$ with the

macroscopic wave function ψ_m in the Heisenberg equation of motion:

$$i\hbar \frac{\partial \psi_{\pm 1}}{\partial t} = \left(-\frac{\hbar^2}{2M} \nabla^2 + V_{\text{trap}} + q + c_0 \rho \right) \psi_{\pm 1} + c_1 \left(\frac{1}{\sqrt{2}} F_{\mp} \psi_0 \pm F_z \psi_{\pm 1} \right), \quad (42a)$$

$$i\hbar \frac{\partial \psi_0}{\partial t} = \left(-\frac{\hbar^2}{2M} \nabla^2 + V_{\text{trap}} + c_0 \rho \right) \psi_0 + \frac{c_1}{\sqrt{2}} (F_+ \psi_1 + F_- \psi_{-1}), \quad (42b)$$

where ρ and \mathbf{F} are defined using ψ_m instead of $\hat{\psi}_m$ in Eqs. (3) and (4). The wave function is normalized as

$$\int d\mathbf{r} \sum_{m=-1}^1 |\psi_m|^2 = N, \quad (43)$$

with N being the number of atoms in the condensate.

Suppose that all atoms are initially in the $m = 0$ state. It follows then from Eq. (42a) that $\psi_{\pm 1}$ will remain zero in the subsequent time evolution. This is because quantum fluctuations in the transverse magnetization that trigger the growth of magnetization are neglected in the mean-field approximation. We therefore introduce an appropriate initial noise in $\psi_{\pm 1}$ so that the mean-field approximation reproduces the quantum evolution.

Let us write the initial state as

$$\psi_{\pm 1}(\mathbf{r}) = \sum_{\mathbf{k}} \frac{1}{\sqrt{V}} e^{i\mathbf{k}\cdot\mathbf{r}} a_{\pm 1, \mathbf{k}}(0), \quad (44)$$

where $a_{\pm 1, \mathbf{k}}$ are c-numbers. We assume that the c-number amplitudes $a_{\pm 1, \mathbf{k}}(0)$ are stochastic variables whose average values vanish,

$$\langle a_{\pm 1, \mathbf{k}}(0) \rangle_{\text{avg}} = 0, \quad (45)$$

where by $\langle \dots \rangle_{\text{avg}}$ we denote the statistical average over an appropriate probability distribution. The linear approximation of the GP equation with respect to $a_{\pm 1, \mathbf{k}}$ gives the same time evolution as Eq. (11), in which the operators are replaced by the c-numbers. We thus obtain

$$F_+(\mathbf{r}, t) F_-(\mathbf{r}', t) = \frac{2n}{V} \sum_{\mathbf{k}} \left| \cos \frac{E_k t}{\hbar} + i \frac{\varepsilon_k + q}{E_k} \sin \frac{E_k t}{\hbar} \right|^2 \times \left[e^{-i\mathbf{k}\cdot(\mathbf{r}-\mathbf{r}')} |a_{1, \mathbf{k}}(0)|^2 + e^{i\mathbf{k}\cdot(\mathbf{r}-\mathbf{r}')} |a_{-1, -\mathbf{k}}(0)|^2 \right]. \quad (46)$$

Comparing Eq. (46) with Eq. (17a), we find that they have the same form if the variance of $a_{\pm 1, \mathbf{k}}(0)$ satisfies

$$\langle |a_{\pm 1, \mathbf{k}}(0)|^2 \rangle_{\text{avg}} = \frac{1}{2} \quad (47)$$

for all \mathbf{k} .

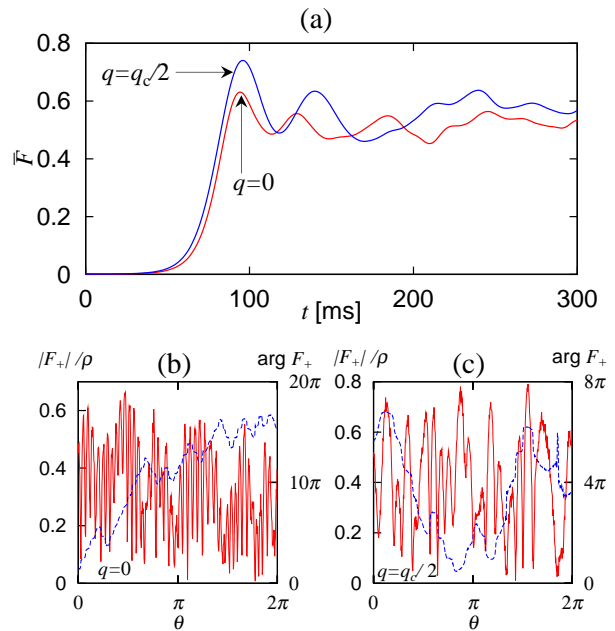


FIG. 1: (Color online) (a) Time evolution of the auto correlation function given in Eq. (49) for the 1D ring geometry. (b) Magnitude of the normalized magnetization $|F_+|/\rho$ (solid curve, left axis) and direction of the magnetization $\arg F_+$ (dashed curve, right axis) at $t = 70$ ms for $q = 0$ and (c) for $q = q_c/2$. The radius of the ring is $R = 50 \mu\text{m}$, the atomic density is $n = 2.8 \times 10^{14} \text{ cm}^{-3}$, and the number of atoms is $N = 10^6$.

In the following, we will perform numerical simulation of spontaneous magnetization using the GP equation and show that the ensuing dynamics exhibits defect formation similar to the KZ mechanism. As the initial state of the $m = \pm 1$ wave functions, we use Eq. (44) with

$$a_{\pm 1, \mathbf{k}}(0) = \alpha_{\text{rnd}} + i\beta_{\text{rnd}}, \quad (48)$$

where α_{rnd} and β_{rnd} are random variables following the normal distribution $p(x) = \sqrt{2/\pi} \exp(-2x^2)$. Equation (48) then satisfies Eqs. (45) and (47).

B. 1D ring geometry

Let us first investigate the 1D ring system. Experimentally this geometry can be realized, e.g., by an optical trap using a Laguerre-Gaussian beam [19]. We reduce the GP equation (42) to 1D by assuming that the wave function ψ_m depends only on the azimuthal angle θ . The average density of atoms is assumed to be $n = 2.8 \times 10^{14} \text{ cm}^{-3}$. When the radius of the ring is $R = 50 \mu\text{m}$ and the radius of the small circle is $2 \mu\text{m}$, the total number of atoms is $N \simeq 10^6$.

Figure 1 illustrates a single run of time evolution for an initial state given by Eqs. (44) and (48). Figure 1

(a) shows time evolution of the auto correlation function defined by

$$\bar{F}(t) = \int R d\theta \frac{|F_+(\theta, t)|^2}{\rho^2(\theta, t)}. \quad (49)$$

For both $q = 0$ and $q = q_c/2$, the transverse magnetization grows exponentially with a time constant $\sim \tau = \hbar/q_c \simeq 8$ ms. Snapshots of the transverse magnetization at $t = 70$ ms are shown in Figs. 1 (b) and 1 (c) for $q = 0$ and $q = q_c/2$, respectively. We define the spin winding number as

$$w = \frac{1}{2\pi} \int_0^{2\pi} R d\theta \frac{1}{2i|F_+|^2} \left(F_- \frac{\partial F_+}{\partial \theta} - F_+ \frac{\partial F_-}{\partial \theta} \right), \quad (50)$$

which represents the number of rotation of the spin vector in the x - y plane along the circumference, and of course w is an integer. The spin winding numbers are $w = 7$ in Fig. 1 (b) and $w = -1$ in Fig. 1 (c).

Figure 2 (a) shows the ensemble average of the normalized correlation function,

$$\langle F_{\text{corr}}(\delta\theta) \rangle_{\text{avg}} = \left\langle \frac{\int d\theta F_+(\theta) F_-(\theta + \delta\theta)}{\int d\theta \rho(\theta) \rho(\theta + \delta\theta)} \right\rangle_{\text{avg}}, \quad (51)$$

at $t = 70$ ms. For $q = q_c/2$, the correlation function has the characteristic width of $\sim \Xi$ in Eq. (23), indicating that the ring is filled with magnetic domains with an average size of $\sim \Xi$. According to the KZ theory, the magnetic domains with random directions give rise to the spin winding, which is estimated to be $w \sim (R/\Xi)^{1/2}$. This R dependence of w is clearly seen in Fig. 2 (b). The ensemble average of the winding number, $\langle w \rangle_{\text{avg}}$, vanishes due to the random nature of the initial noise, and the square root of its variance, $\langle w^2 \rangle_{\text{avg}}^{1/2}$, should be regarded as a typical winding number. The variance is expected to obey the χ^2 distribution with 1000 degrees of freedom, and hence we show the 95% confidence interval to estimate the statistical errors in Fig. 2. As shown in the inset of Fig. 2 (b), the typical winding number changes in time, since the ferromagnetic energy is converted to the kinetic energy and the system exhibits complicated dynamics.

The situation is different for $q = 0$, in which the correlation function oscillates with a Gaussian envelope as shown in Fig. 2 (a). This form of the correlation function gives us the answer to the question as to how the KZ mechanism manifests itself in spin conserving systems. The finite correlation length for $q = 0$ indicates that the spin is conserved not only globally but also locally, that is, the locally integrated spin over the correlation length ξ ,

$$\int_{|\delta\mathbf{r}| \lesssim \xi} \mathbf{F}(\mathbf{r} + \delta\mathbf{r}) d\delta\mathbf{r}, \quad (52)$$

is held to be zero for any \mathbf{r} . This local spin conservation is due to formation of staggered domain or helical spin structures whose periodic length is much smaller than

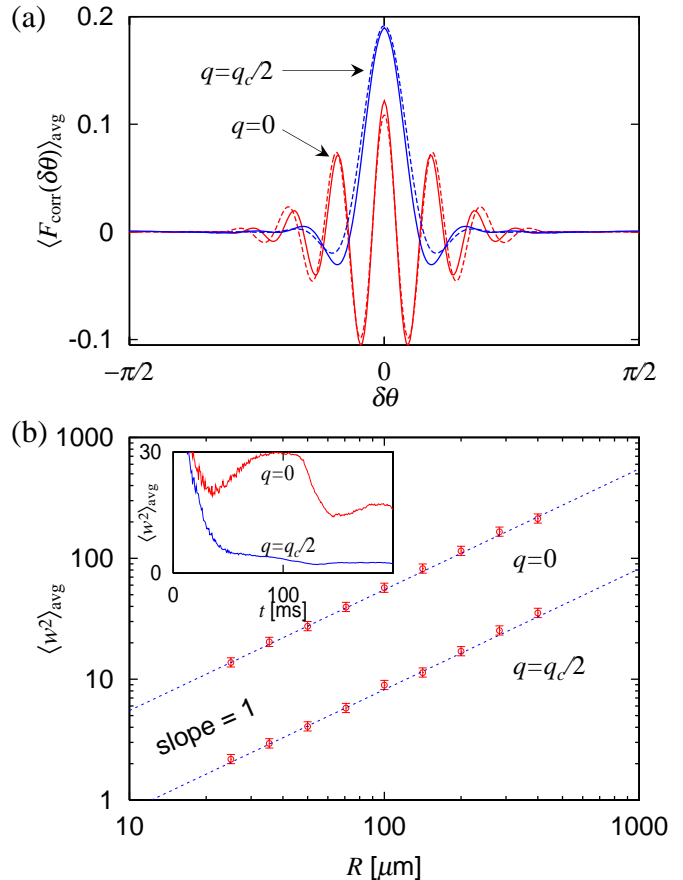


FIG. 2: (Color online) (a) Numerically obtained correlation function given in Eq. (51) at $t = 70$ ms (solid curves), and theoretical fits (dashed curves) from Eqs. (24) and (26). Other parameters are the same as those in Fig. 1. (b) R dependence of the variance of the spin winding number, where the number of atoms is related to R as $N = 10^6 \times R [\mu\text{m}] / 50$. The dashed lines are semi-log fits to the numerical data. The inset shows the time dependence of $\langle w^2 \rangle_{\text{avg}}$ for $R = 50 \mu\text{m}$. The data in (a) and (b) are averages over 1000 runs of simulations for different initial states produced by random numbers. The error bars in (b) represent the 95% confidence interval of the χ^2 distribution.

ξ . Thus, the neighboring domains tend to have opposite magnetizations to cancel out the spin locally, and the domains far from each other grow independently; the spin conservation and the KZ mechanism are thus compatible.

The oscillation in the correlation function originates from the fact that the most unstable modes have nonzero wave numbers $\pm k_{\text{mu}}$. Each correlated region of size $\sim \xi = [8\hbar^2/(Mq_c)]^{1/2}$ contains spin waves of $e^{ik_{\text{mu}}R\theta}$ and $e^{-ik_{\text{mu}}R\theta}$. If there is an imbalance between these modes, the winding number monotonically increases or decreases in each region of $\sim \xi$. This is the reason why $\langle w^2 \rangle_{\text{avg}}$ is larger for $q = 0$ than for $q = q_c/2$ in Fig. 2 (b). It follows from this consideration that for $k_{\text{mu}}\xi \gg 1$ the winding

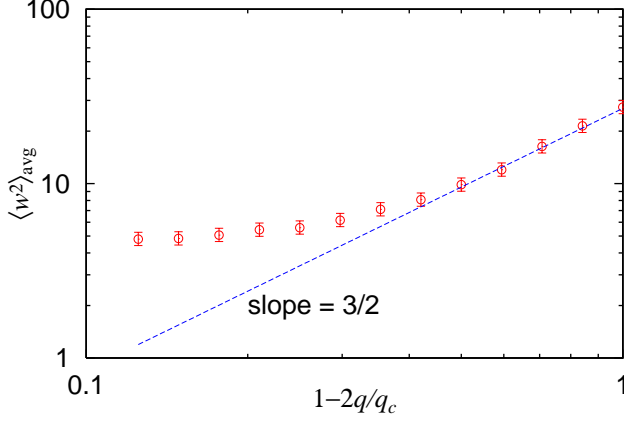


FIG. 3: (Color online) Dependence of the variance of the spin winding number on q . Except for q , the parameters are the same as those in Fig. 1. The dashed line is proportional to $(1 - 2q/q_c)^{3/2}$. The plots show the averages over 1000 runs of simulations for different initial states produced by random numbers. The error bars represent the 95% confidence interval of the χ^2 distribution.

number is proportional to

$$w \sim k_{\text{mu}} \xi \sqrt{\frac{R}{\xi}} = k_{\text{mu}} \sqrt{R\xi} \propto \left(1 - \frac{2q}{q_c}\right)^{3/4}, \quad (53)$$

where Eqs. (14) and (20) are used. Figure 3 shows the averaged variance of the winding number versus $1 - 2q/q_c$. For small q , $\langle w^2 \rangle_{\text{avg}}$ is proportional to $(1 - 2q/q_c)^{3/2}$, in agreement with Eq. (53). When q is close to $q_c/2$, the spin winding within the correlated region, $k_{\text{mu}}\xi$, becomes small, and then the winding number reduces to the value shown in Fig. 2 (b), i.e., $\langle w^2 \rangle_{\text{avg}} \simeq 4$.

We next discuss the results of simulations of slow quench as in Eq. (30). Since the winding number for the slow quench is small compared with the fast quench, we take a large ring of $R = 400 \mu\text{m}$. Figure 4 shows the variance of the winding number as a function of the quench time. We can clearly see that $\langle w^2 \rangle_{\text{avg}}$ has a power law of $\tau_Q^{-1/3}$ within the statistical error, which is in agreement with $\xi_Q^{-1} \sim \tau_Q^{-1/3}$, with ξ_Q being given in Eq. (38). Thus, the present system follows the quench-time scaling of Zurek [2]. We note that, in the slow quench, the winding number converges to an almost constant value for varying quench time τ_Q , as shown in the inset of Fig. 4. This is because little excess energy other than for exciting spin vortices is available for the slow quench.

C. 2D disk geometry

When the confinement in the z direction is tight, the system is effectively 2D. For simplicity, we ignore the density dependence in the z direction, and assume that the

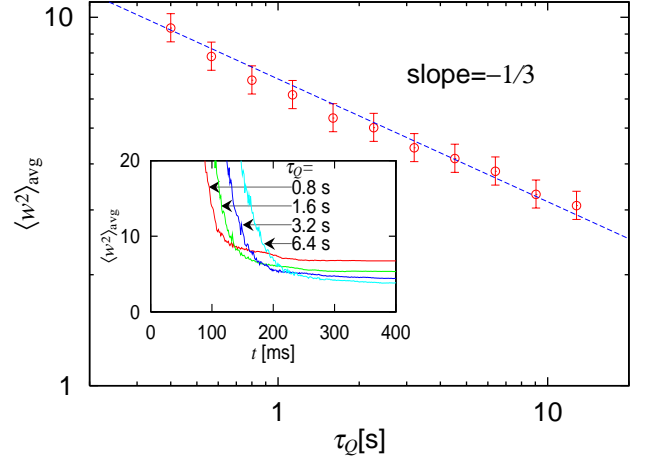


FIG. 4: (Color online) Dependence of the variance of the spin winding number at $t = 400$ ms on the quench time τ_Q , where q is varied as in Eq. (30). The radius of the ring is $R = 400 \mu\text{m}$, the atomic density is $n = 2.8 \times 10^{14} \text{ cm}^{-3}$, and the number of atoms is $N = 8 \times 10^6$. The dashed line is proportional to $\tau_Q^{-1/3}$. The inset shows time evolution of $\langle w^2 \rangle_{\text{avg}}$. The data are averages over 1000 runs of simulations for different initial states produced by random numbers. The error bars represent the 95% confidence interval of the χ^2 distribution.

2D GP equation has the same form as Eq. (42). We assume that the wave function vanishes at the wall located at $(x^2 + y^2)^{1/2} = R_w = 100 \mu\text{m}$, and that the potential is flat inside of the wall. Then the density $n = 2.8 \times 10^{14} \text{ cm}^{-3}$ is almost constant except within the healing length $\{3/[8\pi n(a_0 + 2a_2)]\}^{1/2} \simeq 0.16 \mu\text{m}$ near the wall. When the thickness in the z direction is $\simeq 1 \mu\text{m}$, the number of atoms is $N \simeq 10^7$. Such a system will be realized using an optical sheet and a hollow laser beam.

The initial state of ψ_0 is a stationary solution of the GP equation, and the initial state of $\psi_{\pm 1}$ is given by Eq. (44) with random variables (48). Figure 5 (a) shows time evolution of the autocorrelation function of the transverse magnetization,

$$\bar{F}(t) = \int d\mathbf{r} \frac{|F_+(\mathbf{r}, t)|^2}{\rho^2(\mathbf{r}, t)}, \quad (54)$$

which grows exponentially with the same time constant as that in Fig. 1, and saturates for $t \gtrsim 100$ ms.

Snapshots of $|F_+(\mathbf{r})|$ and $\arg F_+(\mathbf{r})$ at $t = 100$ ms are shown in Figs. 5 (b) and 5 (c). We see that $|F_+(\mathbf{r})|$ at $t \gtrsim 100$ ms contains many holes, around which the spin direction rotates by 2π . Since this topological spin structure consists of singly-quantized vortices in the $m = \pm 1$ states filled by atoms in the $m = 0$ state, it is called the ‘‘polar-core vortex.’’ We can estimate the spin healing length ξ_s by equating the kinetic energy $\hbar^2/(2M\xi_s^2)$ with

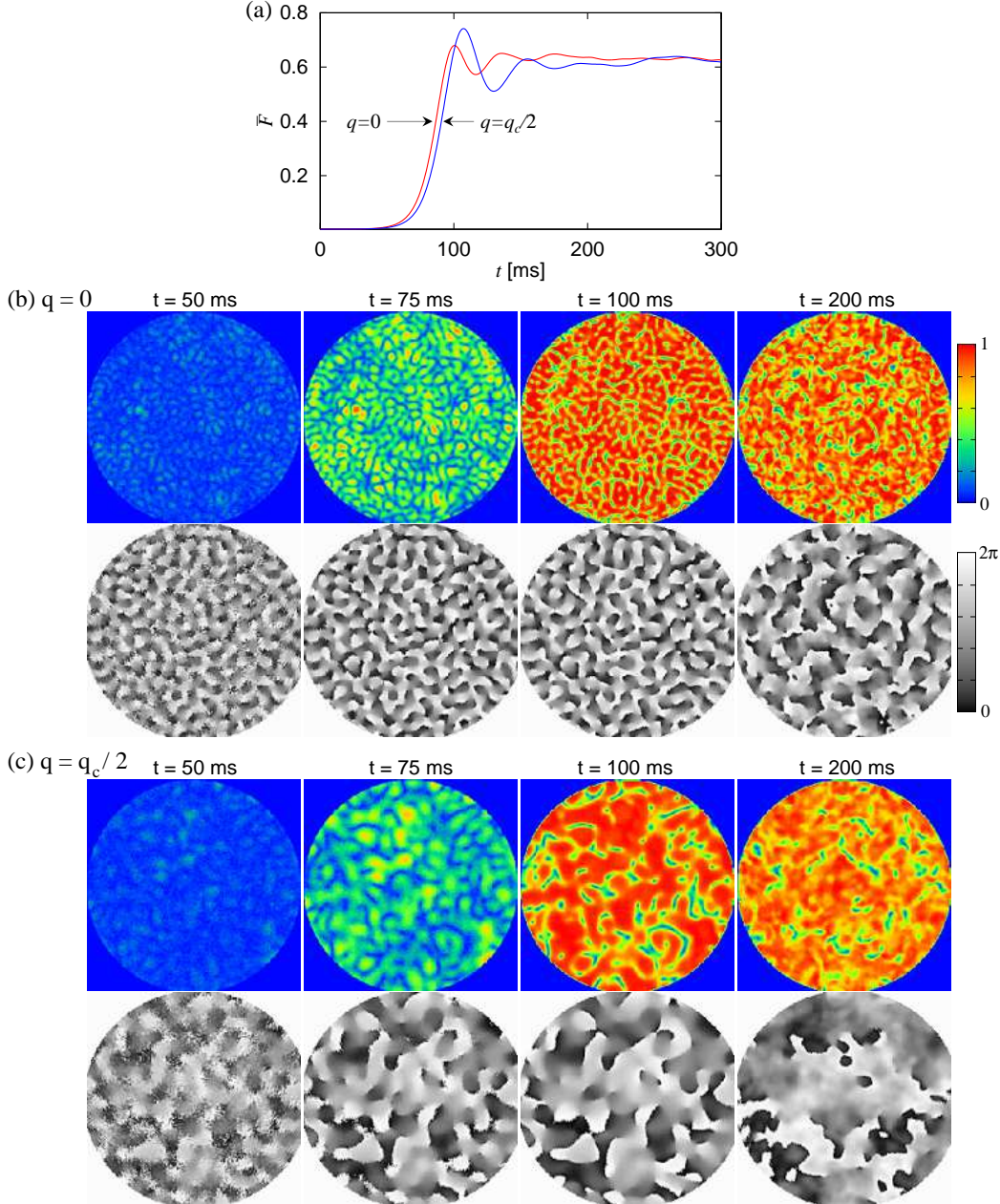


FIG. 5: (Color) (a) Time evolution of the autocorrelation function given in Eq. (54) for the 2D disk geometry. The radius of the disk is $R_w = 100 \mu\text{m}$, the atomic density is $n = 2.8 \times 10^{14} \text{ cm}^{-3}$, and the number of atoms is $N = 10^7$. (b) Profiles of the magnetization $|F_+|$ (upper) and its direction $\arg F_+$ (lower) for $q = 0$ and (c) for $q = q_c/2$. The size of each panel is $200 \mu\text{m} \times 200 \mu\text{m}$.

the energy of magnetization $|q - q_c|$, giving

$$\xi_s = \frac{\hbar}{\sqrt{2M|q - q_c|}}. \quad (55)$$

This length scale is $\xi_s \simeq 1.7 \mu\text{m}$ for $q = 0$ and $\xi_s \simeq 2.4 \mu\text{m}$ for $q = q_c/2$, which are in good agreement with the sizes of the vortex cores in Figs. 5 (b) and 5 (c).

In 2D, the correlation function is defined by

$$\langle F_{\text{corr}}(\delta\mathbf{r}) \rangle_{\text{avg}} = \left\langle \frac{\int d\mathbf{r} F_+(\mathbf{r}) F_-(\mathbf{r} + \delta\mathbf{r})}{\int d\mathbf{r} \rho(\mathbf{r}) \rho(\mathbf{r} + \delta\mathbf{r})} \right\rangle_{\text{avg}}, \quad (56)$$

which are shown in Figs. 6 (a) and 6 (b). We find that as in the 1D case the most unstable wave length is reflected in the shape of the spin correlation function (56), and the characteristics of these correlation functions in the ra-

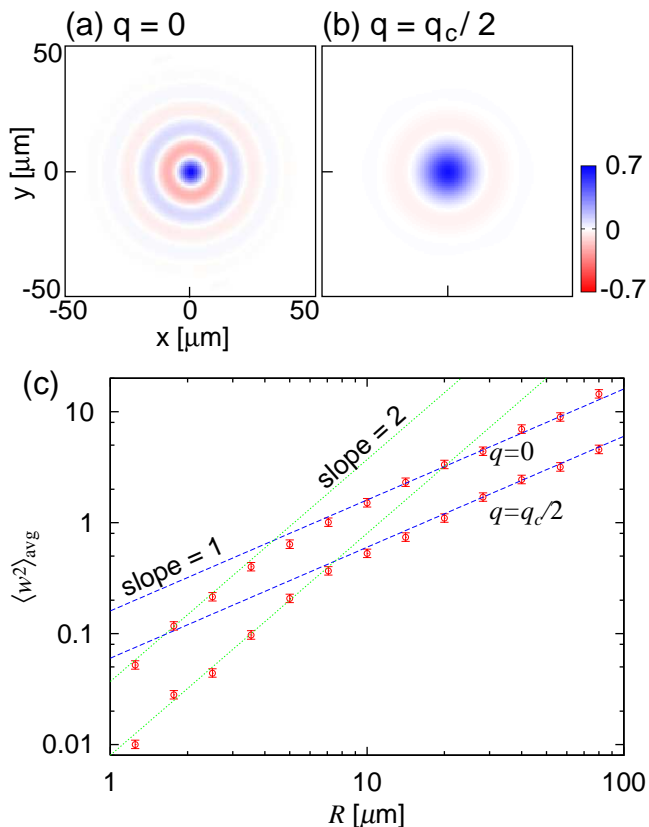


FIG. 6: (Color) (a) Spin correlation function defined in Eq. (56) at $t = 100$ ms for $q = 0$ and (b) for $q = q_c/2$. (c) The variance of the winding number along the circumference of the circle of radius R . The dashed lines and dotted lines are proportional to R and R^2 , respectively. In (a)-(c) the parameters are the same as those in Fig. 5, and the data are averages over 1000 runs of simulations for different initial states produced by random numbers. The error bars in (c) represent the 95% confidence interval of the χ^2 distribution.

dial direction are similar to those in 1D shown in Fig. 2. For $q = 0$, the mean distance between spin vortices in Fig. 5 (b) is not determined by the correlation length (the whole width of the concentric pattern in Fig. 6 (a)) but by $\sim k_{\text{mu}}^{-1}$, i.e., the width of the concentric rings in Fig. 6 (a). On the other hand, for $q = q_c/2$, the density of spin vortices is determined by the correlation length, i.e., the size of the blue circle $\simeq 30 \mu\text{m}$ in Fig. 6 (b). The staggered concentric correlation for $q = 0$ suggests that the spin is conserved locally within the region of the correlation length, and domains at a distance larger than the correlation length grow independently, while conserving the total spin.

The spin winding number for 2D is defined as

$$w(R) = \frac{1}{2\pi} \oint_{C(R)} \frac{1}{2i|F_+|^2} (F_- \nabla F_+ - F_+ \nabla F_-) \cdot d\mathbf{r}, \quad (57)$$

where $C(R)$ is a circle with radius $R < R_w$ located at the center of the system. Figure 6 (c) shows the R depen-

dence of the ensemble average of $w^2(R)$, where the radius of the system is fixed to $R_w = 100 \mu\text{m}$ and the data are taken at $t = 100$ ms. It should be noted that $\langle w^2(R) \rangle_{\text{avg}}$ is proportional to R for large R , as expected from the KZ theory [2], while it is proportional to R^2 for small R . This R^2 dependence is due to the fact that the probability P for a spin vortex to be in the circle is proportional to πR^2 . The variance of the winding number is therefore $0(1-P) + 1^2 P/2 + (-1)^2 P/2 \propto R^2$, if the probability that two or more vortices enter the circle is negligible. This condition is met when the density of spin vortices times πR^2 is much smaller than unity, and hence the radius R at which the crossover from $\langle w^2(R) \rangle_{\text{avg}} \propto R$ to $\propto R^2$ occurs is larger for $q = q_c/2$ than for $q = 0$. As in 1D, nonzero k_{mu} enhances the winding of magnetization, and the winding number is larger for $q = 0$ than for $q = q_c/2$.

Figures 5 (b) and 5 (c) obviously show that the density of spin vortices is uniform when the size of the system is large enough. The number of spin vortices in a radius R is therefore proportional to R^2 . If the topological charge of each spin vortex, $+1$ or -1 , was chosen at random, the net winding number along the circle of radius R , i.e., the difference between the numbers of $+1$ and -1 vortices would be proportional to R . However, from Fig. 6 (c), the winding number is proportional to $R^{1/2}$ for large R , consistent with the KZ mechanism. The topological charge of each spin vortex is thus not at random but anticorrelated to each other to reduce the net winding number.

Figure 7 shows the result of the slow quench for 2D, where $q(t)$ is given by Eq. (30). The winding number follows the scaling law, $\langle w^2 \rangle_{\text{avg}} \propto \tau_Q^{-1/3}$, as predicted from Eq. (38), indicating that Zurek's discussion is applicable also to 2D. In order to obtain this scaling law, we must specify the time at which the winding number is taken, since the spin winding number decays in time, as shown in the inset of Fig. 7. From the scaling law in Eq. (37), we specify the time to take the winding number as

$$\frac{t}{\tau_Q^{1/3}} \left(\frac{q_c}{\hbar} \right)^{2/3} = \text{const.}, \quad (58)$$

which is indicated by the arrows in the inset of Fig. 7.

IV. CONCLUSIONS

In this paper, we have studied the dynamics of a spin-1 BEC with a ferromagnetic interaction after quench of the applied magnetic field in an attempt to investigate spontaneous defect formation in the spinor BEC. We have analyzed the magnetization triggered by quantum fluctuations using the Bogoliubov approximation, and performed numerical simulations of the GP equation with initial conditions that simulate quantum fluctuations.

We have shown that the correlation functions of the magnetization have finite correlation lengths (Figs. 2, 6 (a), and 6 (b)), and therefore magnetic domains far from

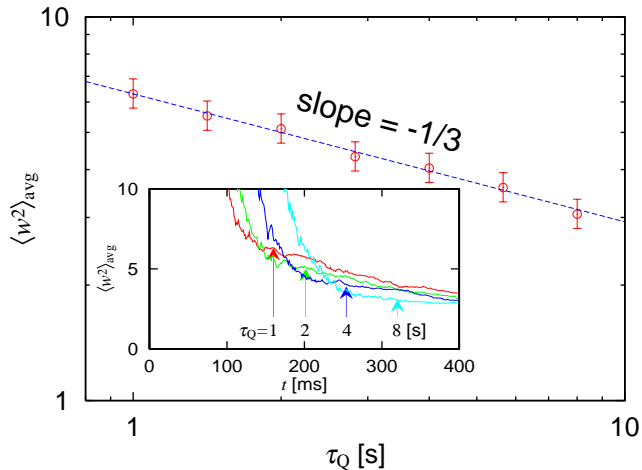


FIG. 7: (Color online) (a) Variance of the spin winding number versus the quench time τ_Q for the 2D disk geometry, where q is varied as in Eq. (30). The inset shows time evolution of $\langle w^2 \rangle_{\text{avg}}$. The plots are taken at the times when $t/\tau_Q^{1/3} = \text{constant}$ is satisfied, which are shown by the arrows in the inset. The dashed line is proportional to $\tau_Q^{-1/3}$. The radius of the disk is $R_w = 400 \mu\text{m}$ and the closed path for taking the winding number is $R = 320 \mu\text{m}$. The atomic density is $n = 2.8 \times 10^{14} \text{cm}^{-3}$ and the number of atoms is $N = 1.6 \times 10^8$. The data are averages over 1000 runs of simulations for different initial states produced by random numbers. The error bars represent the 95% confidence interval of the χ^2 distribution.

each other grow in random directions. We find that topological defects — spin vortices — emerge through the KZ mechanism. We have confirmed that the winding number along the closed path is proportional to the square root of the length of the path (Figs. 2 (b) and 6 (c)), indicating that the topological defects are formed from domains with random directions of magnetizations.

Even when the total magnetization is conserved for $q = 0$, the winding number has the same dependence on the length of the path (Fig. 2 (b)). This is due to the fact that domains within the correlation length tend to be aligned in such a manner as to cancel out local magnetization, and consequently the total magnetization is conserved. Thus, the neighboring domains have local cor-

relation, while domains far from each other are independent, which makes the KZ mechanism compatible with the total spin conservation. The formation of the local correlation also creates topological defects as well as the KZ mechanism, and the winding number exhibits the q dependence as shown in Fig. 3.

When the magnetic field is quenched in finite time τ_Q as in Eq. (30), the winding number has been shown to be proportional to $\tau_Q^{-1/6}$ (Figs. 4 and 7). This τ_Q dependence of the winding number can be understood from Zurek’s simple discussion [2]: the domains are frozen at which the spin relaxation time becomes the same order of elapsed time.

In the Berkeley experiment [12], the system is an elongated quasi-2D geometry, and not suitable for testing the KZ mechanism. The KZ mechanism should apply to the system in which the size of the system in the x direction is made much larger. In this case, the harmonic potential may affect the scaling law, which merits further study. Moreover in the experiment, from the analysis in Ref. [13], there are some initial atoms in the $m = \pm 1$ components with long-range correlation, which play a role of seeds for large domains and hinder the observation of the KZ mechanism. If the residual atoms in the $m = \pm 1$ components is eliminated completely, magnetization is triggered by quantum fluctuations as shown in the present paper. Another way to remove the effect of the residual atoms may be applying random phases to the $m = \pm 1$ states to erase the initial correlation.

Note added. After our work was completed, the preprint by Damski and Zurek [20] appeared, which performs 1D simulations of the quench dynamics of a spin-1 BEC.

Acknowledgments

This work was supported by Grants-in-Aid for Scientific Research (Grant Nos. 17740263 and 17071005) and by the 21st Century COE programs on “Coherent Optical Science” and “Nanometer-Scale Quantum Physics” from the Ministry of Education, Culture, Sports, Science and Technology of Japan. MU acknowledges support by a CREST program of the JST.

[1] T. W. B. Kibble, J. Phys. A **9**, 1387 (1976).
 [2] W. H. Zurek, Nature (London) **317**, 505 (1985); Phys. Rep. **276**, 177 (1996).
 [3] I. Chuang, R. Durrer, N. Turok, and B. Yurke, Science **251**, 1336 (1991).
 [4] M. J. Bowick, L. Chandar, E. A. Schiff, and A. M. Srivastava, Science **263**, 943 (1994).
 [5] P. C. Hendry, N. S. Lawson, R. A. M. Lee, P. V. E. McClintock, and C. D. H. Williams, Nature (London) **368**, 315 (1994); M. E. Dodd, P. C. Hendry, N. S. Lawson,

P. V. E. McClintock, and C. D. H. Williams, Phys. Rev. Lett. **81**, 3703 (1998).
 [6] V. M. H. Ruutu, V. B. Eltsov, A. J. Gill, T. W. B. Kibble, M. Krusius, Yu. G. Makhlin, B. Plaças, G. E. Volovik, and W. Xu, Nature (London) **382**, 334 (1996); V. M. Ruutu, V. B. Eltsov, M. Krusius, Yu. G. Makhlin, B. Plaças, and G. E. Volovik, Phys. Rev. Lett. **80**, 1465 (1998).
 [7] C. Bäuerle, Yu. M. Bunkov, S. N. Fisher, H. Godfrin, and G. R. Pickett, Nature (London) **382**, 332 (1996).

- [8] S. Ducci, P. L. Ramazza, W. González-Viñas, and F. T. Arecchi, *Phys. Rev. Lett.* **83**, 5210 (1999).
- [9] R. Carmi, E. Polturak, and G. Koren, *Phys. Rev. Lett.* **84**, 4966 (2000).
- [10] R. Monaco, J. Mygind, and R. J. Rivers, *Phys. Rev. Lett.* **89**, 080603 (2002).
- [11] A. Maniv, E. Polturak, and G. Koren, *Phys. Rev. Lett.* **91**, 197001 (2003).
- [12] L. E. Sadler, J. M. Higbie, S. R. Leslie, M. Vengalattore, and D. M. Stamper-Kurn, *Nature (London)* **443**, 312 (2006).
- [13] H. Saito, Y. Kawaguchi and M. Ueda, *Phys. Rev. A* **75**, 013621 (2007).
- [14] A. Lamacraft, *cond-mat/0611017*.
- [15] M. Uhlmann, R. Schützhold, and U. R. Fischer, *cond-mat/0612664*.
- [16] H. Saito, Y. Kawaguchi and M. Ueda, *Phys. Rev. Lett.* **96**, 065302 (2006).
- [17] J. Stenger, S. Inouye, D. M. Stamper-Kurn, H. -J. Miesner, A. P. Chikkatur, and W. Ketterle, *Nature (London)* **396**, 345 (1998).
- [18] K. Murata, H. Saito, and M. Ueda, *Phys. Rev. A* **75**, 013607 (2007).
- [19] T. Kuga, Y. Torii, N. Shiokawa, T. Hirano, Y. Shimizu, and H. Sasada, *Phys. Rev. Lett.* **78**, 4713 (1997).
- [20] B. Damski and W. H. Zurek, *arXiv:0704.0440*.